

**REPORT DOCUMENTATION PAGE**

*Form Approved  
OMB No. 0704-0188*

The public reporting burden for this collection of information is estimated to average 1 hour per response, including the time for reviewing instructions, searching existing data sources, gathering and maintaining the data needed, and completing and reviewing the collection of information. Send comments regarding this burden estimate or any other aspect of this collection of information, including suggestions for reducing the burden, to Department of Defense, Washington Headquarters Services, Directorate for Information Operations and Reports (0704-0188), 1215 Jefferson Davis Highway, Suite 1204, Arlington, VA 22202-4302. Respondents should be aware that notwithstanding any other provision of law, no person shall be subject to any penalty for failing to comply with a collection of information if it does not display a currently valid OMB control number.

**PLEASE DO NOT RETURN YOUR FORM TO THE ABOVE ADDRESS.**

1. REPORT DATE (DD-MM-YYYY)		2. REPORT TYPE		3. DATES COVERED (From - To)	
4. TITLE AND SUBTITLE				5a. CONTRACT NUMBER	
				5b. GRANT NUMBER	
				5c. PROGRAM ELEMENT NUMBER	
6. AUTHOR(S)				5d. PROJECT NUMBER	
				5e. TASK NUMBER	
				5f. WORK UNIT NUMBER	
7. PERFORMING ORGANIZATION NAME(S) AND ADDRESS(ES)				8. PERFORMING ORGANIZATION REPORT NUMBER	
9. SPONSORING/MONITORING AGENCY NAME(S) AND ADDRESS(ES)				10. SPONSOR/MONITOR'S ACRONYM(S)	
				11. SPONSOR/MONITOR'S REPORT NUMBER(S)	
12. DISTRIBUTION/AVAILABILITY STATEMENT					
13. SUPPLEMENTARY NOTES					
14. ABSTRACT					
15. SUBJECT TERMS					
16. SECURITY CLASSIFICATION OF:			17. LIMITATION OF ABSTRACT	18. NUMBER OF PAGES	19a. NAME OF RESPONSIBLE PERSON
a. REPORT	b. ABSTRACT	c. THIS PAGE			19b. TELEPHONE NUMBER (Include area code)

## Final Technical Report

Performance period: June 1st 2010 - February 28th 2011

Mathematical Systems & Solutions Inc.  
685 Busch Garden Dr., Pasadena, CA 91105

### 1 Objectives

We seek to produce fast, high-order solvers for geometrically complex configurations containing dielectric/magnetic penetrable scatterers, open and/or closed surfaces as well as perfect and lossy conductors. These are configurations of fundamental importance in diverse fields, with application to (a) Electromagnetic compatibility (EMC), (b) Electromagnetic interference on cavity-bound electronics (EMI), (c) Evaluation of electromagnetic response of dielectric/magnetic coated conductors, and (d) Evaluation of scattering by modern metallic/nonmetallic aircraft structures—amongst many others.

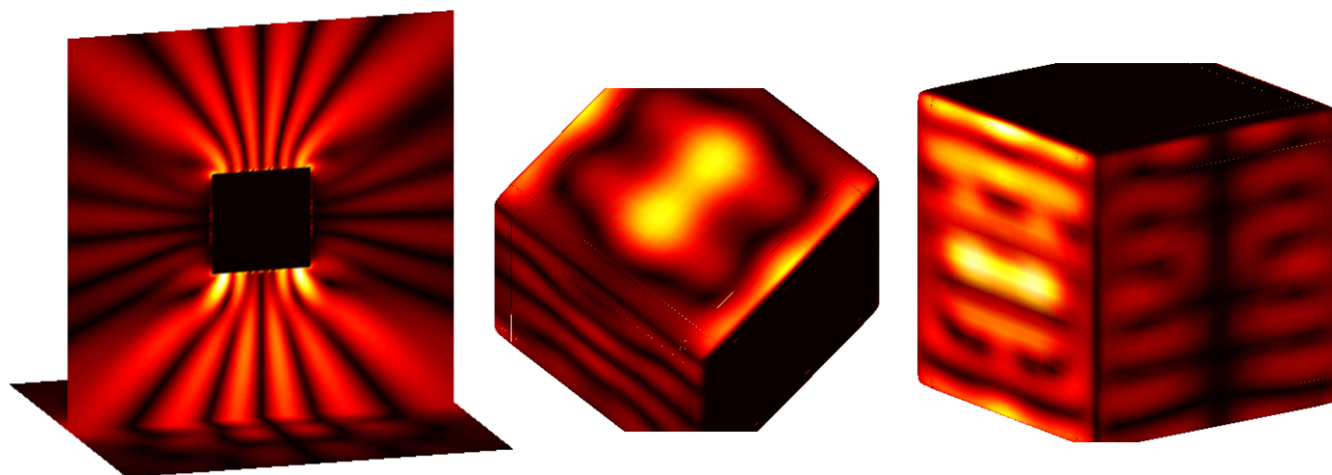


Figure 1: Electromagnetic scattering by a perfectly conducting cubic scatterer (edge-length = 2 under plane-wave,  $k = 20$  normal incidence. Left:  $z$ -component of the electric field. Center and Right:  $x$ - and  $z$ -components of the surface current.

### 2 Accomplishments

Over the nine-month duration of this effort we developed a variety of electromagnetic scattering solvers whose combined use enables solution of a wide range of problems in the field of electromagnetic compatibility. In particular, we 1) Developed surface integral equations for *homogeneous and isotropic dielectric bodies* whose bounding surfaces can contain *corners and edges*, and that incorporate regularizations which give rise to favorable eigenvalue distributions and small numbers of GMRES iterations; 2) Implemented a fast high-order solver for dielectric-body integral equations introduced per point 1 above, for dielectric

bodies containing edges and corners, *allowing for use of overlapping and non-overlapping patches*; 3) Developed new EM scattering solvers for *open metallic surfaces* for scatterers containing edges and corners; 4) Initiated a study to determine the domains of applicability of *impedance boundary conditions* through comparisons with full numerical solutions for thin volumetric conductors; and 5) Produced a new Green-function/Integral-Equation methodology for solution of problems involving two dimensional periodicity in three-dimensional space; see e.g. Figure 2 and Section 2.3. *This is the first approach ever developed that can successfully solve bi-periodic scattering problems in three-dimensional space at and around Wood anomaly frequencies.*

Finally, the qualities of all solvers developed were demonstrated via compelling applications to configurations relevant to the field of electromagnetic compatibility. We feel we have successfully addressed the central objectives laid down on our Phase I proposal. We have recently received an invitation to submit a Phase II proposal; we believe the results of our work over the Phase I effort, which are described in what follows, clearly demonstrate the significant potential and feasibility of the proposed methodologies.

The subsequent Phase II work will proceed to 1) Enable application of the methodologies developed during the Phase I to multi-scale geometries containing a span of length-scales, including configurations such as full aircraft, attachments, associated electronics, etc.; and 2) Produce a user friendly Graphical User Interface that facilitates application of the software infrastructure to relevant engineering configurations.

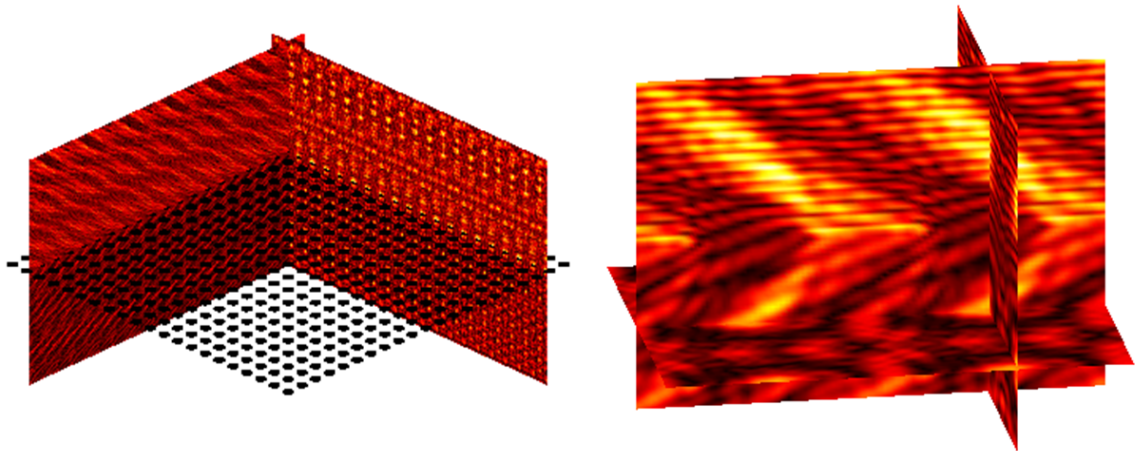


Figure 2: Scattering by an *infinite* bi-periodic array of plates with periods equal to ten point four wavelengths:  $p_1 = p_2 = 10.4\lambda$ . Plane wave incidence, with incidence angle  $\theta = 45^\circ$ . Left:  $21 \times 21$  section of the infinite array and total field (incident plus scattered) on to two coordinate planes. Right: Close-up on the total field around a set of three plates.

## 2.1 Well conditioned integral equation for problems of scattering by dielectric bodies and thin metallic plates

The problem of scattering by dielectrics is governed by Maxwell's equations

$$\text{curl curl } \mathbf{u}^j + k_j^2 \mathbf{u}^j = 0 \quad \text{in the domains } D^j, \quad j = 1, 2$$

for the electromagnetic fields  $\mathbf{u}^j$ ,  $j = 1, 2$  in the (bounded) scatterer  $D^2$  and the surrounding space  $D^1$ , respectively; in what follows we assume the domains  $D^1$  and  $D^2$  are separated by a bounded surface  $\Gamma$ . The material properties of the regions  $D^j$  are characterized by two wave-numbers  $k_j$ . The Maxwell equations are supplemented with (1) transmission boundary conditions on the material interface  $\Gamma$  of the

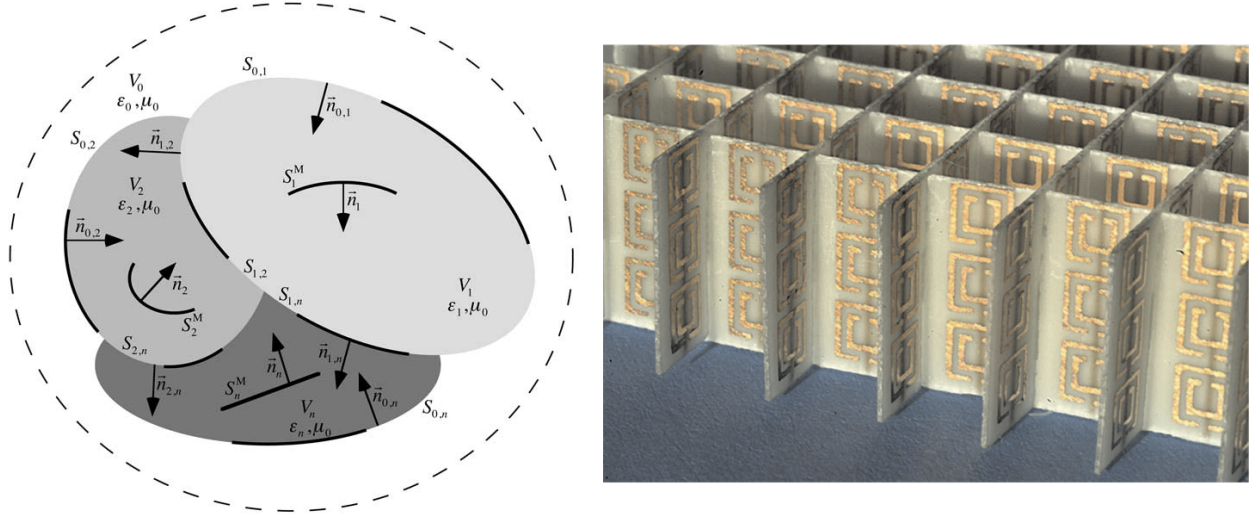


Figure 3: Left. General composite, consisting of a number of penetrable regions containing dielectric/magnetic materials of various permittivities and/or permeabilities, and partially coated by thin metallic surface coatings and/or containing embedded metallic plates or bodies. Right. An example of such a configuration: Pendry's negative index composite. Manifold important applications of the proposed dielectric-metallic electromagnetic solvers exist; see points (a) through (d) above.

form  $\gamma_D^1 \mathbf{u}^1 - \gamma_D^2 \mathbf{u}^2 = -\gamma_D^1 \mathbf{u}^{inc}$  and  $\gamma_N^1 \mathbf{u}^1 - \gamma_N^2 \mathbf{u}^2 = -\gamma_N^1 \mathbf{u}^{inc}$  in terms of the Dirichlet  $\gamma_D^j = \mathbf{n} \times \cdot$  and Neumann traces  $\gamma_N^j = \mathbf{n} \times \text{curl} \cdot$  for an incident field  $\mathbf{u}^{inc}$ , and (2) radiation conditions at infinity on  $\mathbf{u}^1$ . The transmission problem in dielectric materials with bounded interfaces is amenable to a wider variety of boundary integral equation formulations than is the corresponding PEC problem. Among these, integral equations of the second kind have been obtained using subtractive cancellations of the principal parts of hypersingular operators in the form  $\mathcal{T}_1^{PV} - \mathcal{T}_2^{PV}$  (where the operators  $\mathcal{T}_j$  correspond to the wavenumbers  $k_j$ ). However, these formulations become ill-conditioned for low and high-contrast dielectrics (see also our results in Figure 4) and thus are of limited use for a range of applications that involve such material properties (such as, e.g., narrow-band dielectric photonic crystals).

Since the availability of robust integral equation formulations throughout the range of dielectric contrasts is highly desirable for treatment of the types of problems under consideration, we seek to design such formulations on the basis of coercive approximations of the dielectric admittance/capacity operators. The latter operators—reminiscent of the Dirichlet-to-Neumann acoustic operators, and denoted hereby as  $\mathcal{R}^T$ —are defined to map the boundary conditions of the dielectric transmission problems for the field  $\mathbf{u} = (\mathbf{u}^1, \mathbf{u}^2)$ , that is  $\gamma_T(\mathbf{u}) = (\gamma_D^1 - \gamma_D^2; \gamma_N^1 - \gamma_N^2)(\mathbf{u})$  to the Cauchy data of  $\mathbf{u}$  on  $\Gamma$  defined as  $\gamma_C(\mathbf{u}) = (\gamma_D^1 \mathbf{u}^1, \gamma_N^1 \mathbf{u}^1; \gamma_D^2 \mathbf{u}^2, \gamma_N^2 \mathbf{u}^2)$ , and thus  $\mathcal{R}^T \gamma_T = \gamma_C$ . Since the electromagnetic field  $\mathbf{u}$  can be obtained from knowledge of its traces on  $\Gamma$  via the Stratton-Chu formulas in the form  $\mathbf{u}^j = \mathcal{C}_j(\gamma_D^j \mathbf{u}^j, \gamma_N^j \mathbf{u}^j) = (-1)^j (\mathcal{M}_j(\gamma_D^j \mathbf{u}^j) + 1/k_j^2 \mathcal{E}_j(\gamma_N^j \mathbf{u}^j))$ , where  $(\mathcal{M}_j \mathbf{a})(\mathbf{z}) = \text{curl} \int_{\Gamma} G_{k_j}(\mathbf{z} - \mathbf{y}) \mathbf{a}(\mathbf{y}) d\sigma(\mathbf{y})$  and  $(\mathcal{E}_j \mathbf{a})(\mathbf{z}) = \text{curl} \text{curl} \int_{\Gamma} G_{k_j}(\mathbf{z} - \mathbf{y}) \mathbf{a}(\mathbf{y}) d\sigma(\mathbf{y})$ , it follows that  $\gamma_T(\mathcal{C}_1, \mathcal{C}_2) \mathcal{R}^T = I$  on  $\Gamma$ . The main idea of our approach in this context is to seek suitable approximations of the admittance operator  $\mathcal{R}^T$  in the form  $(\tilde{\mathcal{R}}_1^T, I - \tilde{\mathcal{R}}_1^T)$ —where the operator  $\tilde{\mathcal{R}}_1^T$  approximates in a certain sense the operator  $\mathcal{R}_1^T \gamma_T = (\gamma_D^1, \gamma_N^1)$ —and seek for electromagnetic fields  $\mathbf{u}^j$ ,  $j = 1, 2$  in the form

$$\mathbf{u}^1 = [\mathcal{C}_1(\tilde{\mathcal{R}}_1^T)](\mathbf{w}), \quad \mathbf{u}^2 = [\mathcal{C}_2(I - \tilde{\mathcal{R}}_1^T)](\mathbf{w})$$

for an unknown tangential current distribution  $\mathbf{w} = (\mathbf{w}_1, \mathbf{w}_2)$ . The representation presented above for the

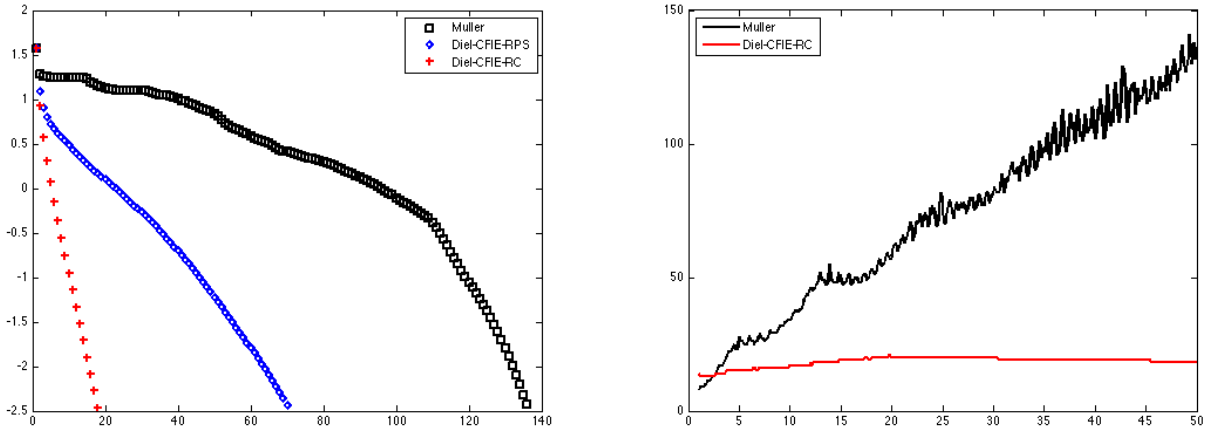


Figure 4: Left: number of GMRES iterations required by the various formulations for the nearly resonant electromagnetic transmission problem,  $\omega = 50$ ,  $\epsilon_1 = 1$ ,  $\epsilon_2 = 2$ , spherical geometries—Diel-CFIE-RC (red), – Diel-CFIE-RPS (blue), – Müller’s CFIE (black); Right: Number of iterations required by each formulation as a function of the frequency  $\omega = 1, 1.1, \dots, 50$ .

fields  $\mathbf{u}^j$ ,  $j = 1, 2$  leads to boundary integral equations of the form

$$[\gamma_T(\mathcal{C}_1, \mathcal{C}_2)(\tilde{\mathcal{R}}_1^T, I - \tilde{\mathcal{R}}_1^T)](\mathbf{w}) = -(\gamma_D^1 \mathbf{u}^{inc}, \gamma_N^1 \mathbf{u}^{inc}). \quad (1)$$

Adopting the approximation convention that  $\tilde{\mathcal{R}} \sim \mathcal{R}$  if the difference  $\tilde{\mathcal{R}} - \mathcal{R}$  is a compact operator, we use the following operator in equation (1)

$$\tilde{\mathcal{R}}_1^T = \frac{1}{k_1^2 + k_2^2} \begin{pmatrix} 2k_2^2(\frac{k_1}{k_2} \mathcal{T}_1 \mathcal{T}_2 - \frac{I}{4}) & i(k_1 \mathcal{T}_1 + k_2 \mathcal{T}_2) \\ ik_1 k_2 (k_1 \mathcal{T}_2 + k_2 \mathcal{T}_1) & 2k_1^2(\frac{k_2}{k_1} \mathcal{T}_1 \mathcal{T}_2 - \frac{I}{4}) \end{pmatrix} \quad (2)$$

whose derivation is based on the pseudo-differential calculus. Taking into account the fact that  $\gamma_T(\mathcal{C}_1, \mathcal{C}_2)$  is the exact inverse of  $\mathcal{R}^T$ , the choice of  $\tilde{\mathcal{R}}_1^T$  in equation (2) will yield regularized integral equations (1) whose spectra will accumulate at 1. Thus, the operators  $\tilde{\mathcal{R}}_1^T$  can be thought of as regularizing operators, and the ensuing integral equations (1) as dielectric CFIE-R formulations. Taking a cue from our recent work [1] on CFIE-R formulations for the PEC case, in the lossless case when the wavenumbers  $k_j$  are real we will complexify them in the form  $k_j \rightarrow k_j + i\epsilon_j$ ,  $\epsilon_j > 0$  in equation (2) in order to obtain coercive operators  $\tilde{\mathcal{R}}_1^T$  which thus render uniquely solvable integral equations (1).

Results of our ongoing effort suggest that significant gains can result from use of our proposed regularized formulations (1). Indeed, in Figure 4 we compare the number of iterations needed for a GMRES residual of  $10^{-4}$  by the classical Müller’s formulations, and the regularized formulations (1) with the electric field operators replaced by their principal symbols in the definition of the regularizing operators  $\tilde{\mathcal{R}}_1^T$ —the resulting formulations are denoted by Diel-CFIE-RPS—and the complexified wavenumbers—the resulting formulations are denoted by Diel-CFIE-RC. Clearly, the Diel-CFIE-RC equations consistently produce significant gains in numbers of iterations throughout the frequency spectrum (Figure 4 right) —about one order of magnitude reductions compared to those required by the classical Müller formulations, *even near resonances*. We anticipate that commensurate gains will be produced in the case of a variety of dielectric configurations of practical interest through the use of our proposed dielectric CFIE-R formulations. Furthermore, our methodologies for open surfaces and for singular geometries allows for a seamless incorporation of the dielectric CFIE-R formulations in the case where the interfaces of material discontinuities exhibit geometric singularities and may contain lossy or lossless metallic components.

In view of the normal and tangential singularities of surface currents for open surfaces, we seek the scattered electric field off an open Perfect Electrically Conducting (PEC) surface  $\Gamma$  in the form

$$\mathbf{E}^s(z) = ik \int_{\Gamma} G_k(|z - y|) W \mathbf{I}(y) ds(y) + \frac{i}{k} \nabla \int_{\Gamma} G_k(|z - y|) \text{div}_{\Gamma}(W \mathbf{I}) ds(y), \quad (3)$$

where  $W$  is a “weight” matrix and where, denoting by  $\mathbf{J}$  the actual surface current and letting  $\mathbf{J} = W \mathbf{I}$  ( $\mathbf{I}$  is a “regularized” bounded surface current and  $W$  carries explicitly the current singularity at the edge), the regularized current  $I$  satisfies the EFIE equation

$$\mathcal{T}_W \mathbf{I} = -\mathbf{n} \times \mathbf{E}^{inc}. \quad (4)$$

Here  $\mathbf{n}$  is the normal to  $\Gamma$ . The weighted integral operator can be written as

$$\mathcal{T}_W \mathbf{I} = \mathcal{S}_W \mathbf{I} + \mathcal{D}_W \mathbf{I} \quad (5)$$

where operators  $\mathcal{S}_W$  and  $\mathcal{D}_W$  are defined as

$$\mathcal{S}_W \mathbf{I} = ik \mathbf{n} \times \int_{\Gamma} G_k(|x - y|) W \mathbf{I}(y) ds(y) \quad (6)$$

and

$$\mathcal{D}_W \mathbf{I} = -\frac{i}{k} \overrightarrow{\text{curl}}_{\Gamma} \int_{\Gamma} G_k(|x - y|) \text{div}_{\Gamma}(W \mathbf{I}) ds(y) \quad (7)$$

respectively. Here, for a scalar field  $F$  defined on the surface  $\Gamma$ ,  $\overrightarrow{\text{curl}}_{\Gamma}$  denotes the operator  $\overrightarrow{\text{curl}}_{\Gamma} F = (\nabla F) \times \mathbf{n}$ .

Let  $\vec{r}(u, v)$  be a local coordinate chart with  $(u, v) \in (0, 1) \times (0, 1)$  such that  $v = 0$  correspond to an open edge. In this case, the unknown density  $\mathbf{I}$  can be decomposed as

$$\mathbf{I} = I^u \vec{r}_u + I^v \vec{r}_v$$

where  $I^u$  and  $I^v$  are the tangential and normal components of the surface current. Given that the tangent and normal components of the solution have singularity of  $O(1/\sqrt{d})$  and  $O(\sqrt{d})$  respectively, where  $d$  denotes the distance to the edge, the choice of weight matrix

$$W = \frac{1}{\omega} \begin{pmatrix} 1 & -\theta \omega^2 \\ 0 & \omega^2 \end{pmatrix} \quad (8)$$

with  $\omega \sim \sqrt{d}$ , and  $\theta = \vec{r}_u \cdot \vec{r}_v / \vec{r}_u \cdot \vec{r}_u$ , that act on tangential and normal components  $(I^u, I^v)^T$  of  $\mathbf{I}$  as a multiplication by the matrix renders  $I^u$  and  $I^v$  smooth.

Before we discuss the numerical method that is used of to solve (4), we note that once the surface current density  $J$  is obtained as a solution of (4), the electric field can be retrieved using equation (3). Also, if we define the electric far field  $\mathbf{E}_{\infty}(\hat{x})$  as

$$\mathbf{E}^s(x) = \frac{e^{ik|x|}}{|x|} (\mathbf{E}_{\infty}(\hat{x}) + \mathcal{O}(|x|^{-1})) \quad (9)$$

then, one can use the expression

$$\mathbf{E}_{\infty}(x) = \frac{ik}{4\pi} \hat{x} \times \int_{\Gamma} e^{-ik\hat{x} \cdot y} (W \mathbf{I}(y) \times \hat{x}) ds(y) \quad (10)$$

for the electric far field computation.

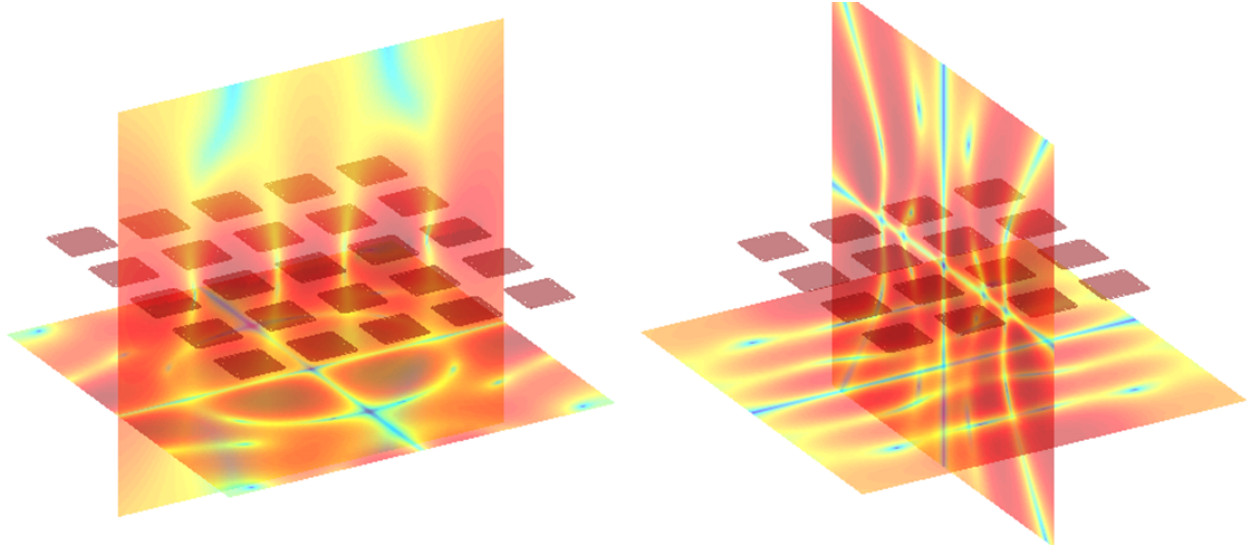


Figure 5: Electromagnetic scattering by a structure made out of an array of  $5 \times 5$  thin metallic surfaces containing corners and edges. (As discussed in the text, related solutions for the significantly simpler *scalar* case were available previous to this work.) The edges are treated by means of the algorithm described in Section 2.2.1, and the corners are modeled by extremely sharp rounded edges, as shown in Figure 6. Structures of this type are ubiquitous amongst the configurations and devices that we seek to treat as part of the present effort; compare Figure 3.

## 2.2 Electromagnetic solvers for open surfaces with corners

These methods build upon previous solvers, which were described as part of our STTR proposal, for *scalar* scattering by open surfaces containing corners. The present solvers provide a significant generalization to the electromagnetic case: the methods and implementations for solution *electromagnetic* scattering by open surfaces containing corners is the result of work associated with the present effort.

The presence of corners in a scattering geometry results in solutions that become unbounded where this blow-up is of different nature from that at open edges. It, thus, poses a significant challenge for the numerical scheme described above in term of achieving high accuracy. In view of this, we adopt a strategy where we solve “nearby” problems on smooth domains that coincide with the original scatterer except in small neighborhoods near the corner. The success of the strategy hinges on its ability to use extremely close approximations of the domains with corners and use of discretization that give rise to solution with limited computational cost. Here, corners have been smoothed via a systematic blending of two arcs on either side of the corner. In the following discussion, we describe the procedure that we adopt to smoothly round these corners. *We emphasize that the procedure is completely general and automatic: it can be applied with ease to a general open surface, with curved edges and associated corners.*

### 2.2.1 Numerical scheme

In this section, we present the main algorithmic components of the numerical scheme that we employ in solving (4), which in turn reduces to accurate evaluations of the weighted integral operator  $\mathcal{T}_W$  and hence  $S_W$  and  $D_W$ .

We note that the accurate evaluation of  $S_W$  in (6) entails obtaining  $(I^u, I^v)^T$  from  $\mathbf{I}$ , which is quite

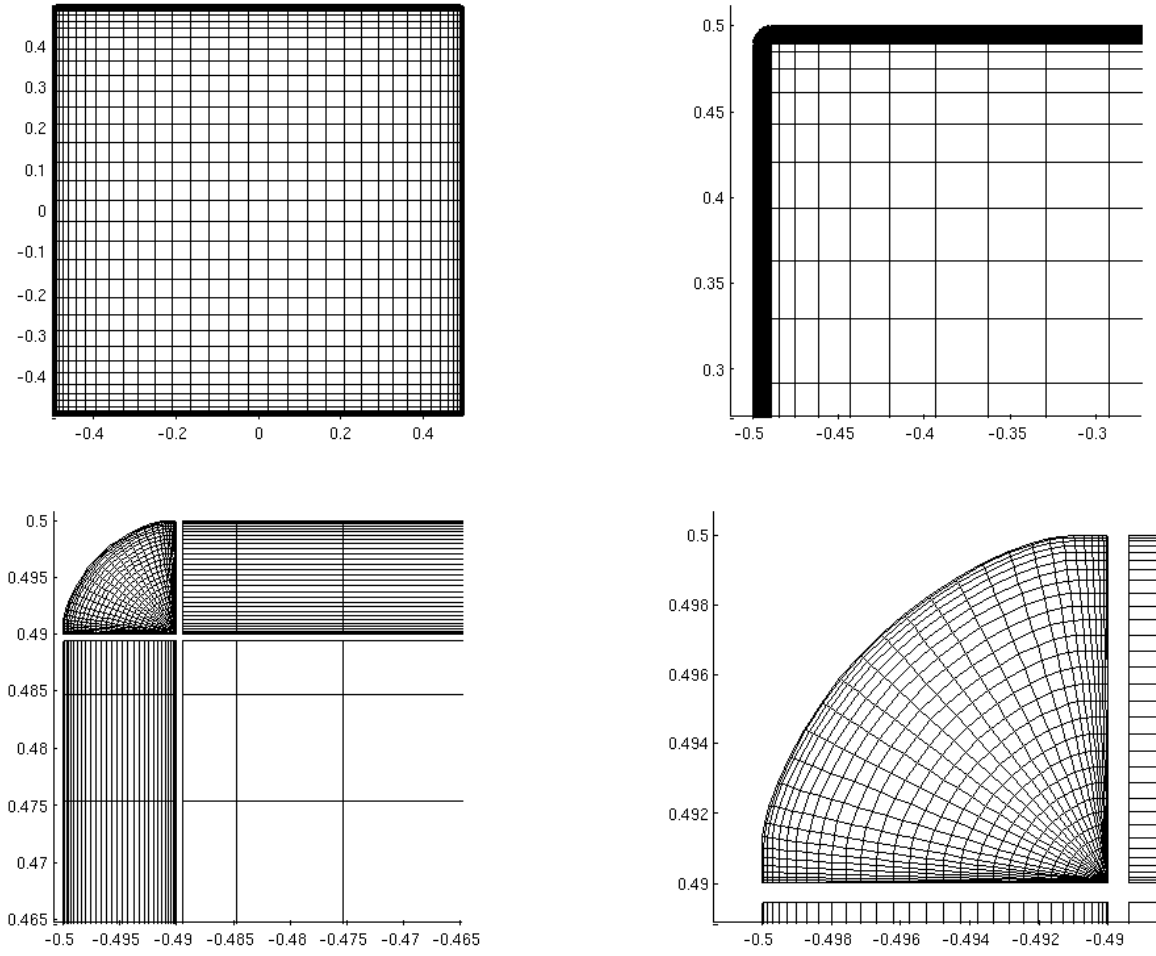


Figure 6: A unit square with smoothly rounded corners. The geometry is divided into interior, edge and corner patches and are discretized as shown above.

straightforward. An application of the  $W$ -matrix on  $(I^u, I^v)^T$  leads to integrals of the form

$$S_\omega[\phi](x) = \int_\Gamma \frac{1}{\omega} G_k(|x-y|) \phi(y) ds(y), \quad (11)$$

where  $\phi$  is smooth, that can then be approximated through a specialized numerical integration method. Toward this end, we employ a high order quadrature that relies on a smooth cut-off function  $\eta_x$  supported in a small neighborhood of the target point  $x$  that is also identically equal to one, i.e.,  $\eta_x \equiv 1$ , in the immediate neighborhood of  $x$ , to split (11) as

$$S_\omega[\phi](x) = \int_{\eta_x \neq 0} \frac{1}{\omega} G_k(|x-y|) \eta_x(y) \phi(y) ds(y) + \int_\Gamma \frac{1}{\omega} G_k(|x-y|) (1-\eta_x(y)) \phi(y) ds(y). \quad (12)$$

Clearly, the second integral in (12) can be accurately approximated using a “Weighted Clenshaw-Curtis” quadrature of the form

$$\int_0^1 \frac{1}{\sqrt{v}} f(v) dv \approx \sum_{n=0}^N w_n f(v_n), \quad (13)$$

where the quadrature points are given by

$$v_n = \frac{1}{2} \left( 1 + \cos \left( \left( n + \frac{1}{2} \right) \frac{\pi}{N} \right) \right)$$

and quadrature weights,  $w_n$ , by

$$w_n = \frac{1}{N} \sum_{m=0}^{N'} - \frac{4}{4m^2 - 1} \cos \left( \left( n + \frac{1}{2} \right) \frac{m\pi}{N} \right)$$

where the primed sum denotes that the first term ( $m = 0$ ) is halved. The first integral in (12), on the other hand, is evaluated by changing to polar coordinates, where  $\rho$ -integrals are performed using a scaled version of (13) and  $\theta$ -integral is evaluated using regular Clenshaw-Curtis quadrature for each piecewise smooth  $\theta$ -interval.

In the evaluation of  $D_W$  in (7), however, care should be taken when dealing with the term  $\text{div}_\Gamma(W\mathbf{I})$  so that the singular weight  $\omega$  gets proper treatment. To this end, we use the formula for the surface divergence in coordinates. For this, we use the fact that for a given tangential field  $\mathbf{X} = X^u \vec{r}_u + X^v \vec{r}_v$  on the patch  $\vec{r}(u, v)$ , the formula for the tangential divergence reads:

$$\text{div}_\Gamma \mathbf{X} = \frac{1}{\sqrt{g}} [\partial_u (\sqrt{g} X^u) + \partial_v (\sqrt{g} X^v)] \quad (14)$$

where  $g = EG - F^2$  is the Riemannian metric tensor, with  $E = \vec{r}_u \cdot \vec{r}_u$ ,  $F = \vec{r}_u \cdot \vec{r}_v$  and  $G = \vec{r}_v \cdot \vec{r}_v$ . A straightforward application of (14) thus yields

$$\begin{aligned} \text{div}_\Gamma(W\mathbf{I}) &= \frac{1}{\omega} \left[ \frac{1}{2g} (\partial_u g (I^u - \theta \omega^2 I^v) + \partial_v g \omega^2 I^v) \right. \\ &\quad \left. + \partial_u I^u - \partial_u \theta \omega^2 I^v - \theta \omega^2 \partial_u I^v + \omega^2 \partial_v I^v + \frac{1}{2} \partial_v (\omega^2) I^v \right] \end{aligned} \quad (15)$$

assuming that  $\omega$  depends only on  $v$ . From the expression in (15), it follows that the integral

$$\int_\Gamma G_k(|x - y|) \text{div}_\Gamma(W\mathbf{I}) ds(y)$$

in (7) has the same form as in (11) and thus can be evaluated using the integration scheme described above.

The last remaining element of our numerical algorithm pertains to derivative computations that arise in (15) as well as in the surface curl differential operator in (7). As these expressions only involve partial derivatives of smooth functions, one can use Chebyshev polynomials as spectrally accurate functional approximations, which can then be used for finite difference approximation of the derivatives of these functions. One can also directly differentiate the approximating Chebyshev series to obtain necessary derivatives. In this case, the loss of accuracy near patch edges can be controlled by restricting the degree of Chebyshev polynomials to a moderate number.

### 2.2.2 Preconditioned Equation

In order to solve better conditioned integral equations, we precondition equation (4) on the left by means of the regularizing operator  $\mathcal{T}_\omega$  defined by

$$\begin{aligned} \mathcal{T}_\omega \mathbf{K} &= ikn \times \int_\Gamma G_k(|x - y|) W \mathbf{K}(y) ds(y) \\ &\quad - \frac{i}{k} \overrightarrow{\text{curl}}_\Gamma \int_\Gamma G_k(|x - y|) \omega(y) \text{div}_\Gamma(\mathbf{K}) ds(y) \\ &= \mathcal{S}_W \mathbf{K} + \mathcal{D}_\omega \mathbf{K}. \end{aligned} \quad (16)$$

More precisely, we solve

$$\mathcal{T}_\omega \circ \mathcal{T}_W(\mathbf{I}) = -\mathcal{T}_\omega(\mathbf{n} \times \mathbf{E}^{inc}) \quad (17)$$

where we express the operator on the left-hand side as

$$\mathcal{T}_\omega \circ \mathcal{T}_W = \mathcal{S}_W \circ \mathcal{S}_W + \mathcal{S}_W \circ \mathcal{D}_W + \mathcal{D}_\omega \circ \mathcal{S}_W. \quad (18)$$

We note that the operator  $\mathcal{D}_\omega$  can be evaluated in a straightforward manner using differentiation and integration methods described in the previous section.

### 2.2.3 Numerical Results

Some of our first results obtained by this methodology are displayed in Figure 6, which shows the solution of a problem of electromagnetic scattering by a structure made out of thin metallic surfaces containing corners and edges. Structures of this type are ubiquitous amongst the configurations and devices that we seek to treat as part of the present effort; compare e.g. Figure 3.

## 2.3 Integral equations based on periodic Green's functions

A variety of integral equations for the electromagnetic transmission and reflection problem exist, including those arising from the Stratton-Chu representation formulas, that express the scattered fields in terms of the physical surface currents. Integral equation formulations of the dielectric scattering problems are posed in terms of the magnetic and electric field integral operators  $\mathcal{K}_k$  and  $\mathcal{T}_k$ , which map tangential fields  $\mathbf{a}$  into tangential fields, and are defined by

$$(\mathcal{K}_k \mathbf{a})(\mathbf{x}) = \mathbf{n}(\mathbf{x}) \times \int_{\Gamma} \nabla_{\mathbf{y}} G_k(\mathbf{x} - \mathbf{y}) \times \mathbf{a}(\mathbf{y}) d\sigma(\mathbf{y}), \quad (19)$$

and

$$\begin{aligned} (\mathcal{T}_k \mathbf{a})(\mathbf{x}) &= ik\mathcal{S}_k \mathbf{a} + \frac{i}{k} \mathcal{T}_k^{\text{PV}} \mathbf{a} = ik\mathbf{n}(\mathbf{x}) \times \int_{\Gamma} G_k(\mathbf{x} - \mathbf{y}) \mathbf{a}(\mathbf{y}) d\sigma(\mathbf{y}) \\ &+ \frac{i}{k} \mathbf{n}(\mathbf{x}) \times \nabla_{\mathbf{x}} \int_{\Gamma} G_k(\mathbf{x} - \mathbf{y}) \text{div}_{\Gamma} \mathbf{a}(\mathbf{y}) d\sigma(\mathbf{y}), \end{aligned} \quad (20)$$

where, in the non-periodic case,  $G_k$  is the outgoing fundamental solution of the Helmholtz equation corresponding to the wavenumber  $k$ ,  $G_k(\mathbf{x}, \mathbf{y}) = G_k(\mathbf{x} - \mathbf{y}) = \frac{e^{ik|\mathbf{x}-\mathbf{y}|}}{4\pi|\mathbf{x}-\mathbf{y}|}$ ; the hyper-singular integral in the definition of  $\mathcal{K}$  should be interpreted in the sense of Cauchy principal value. We denote the corresponding periodic operators, that is, the integral operators arising from the periodic Green's functions by the superscript *per*. Integral equation formulations of periodic dielectric scattering problems assume as unknowns the (interior) magnetic and electric currents  $\mathbf{j}_2 = -\mathbf{n} \times \mathbf{H}^2$  and  $\mathbf{m}_2 = \mathbf{n} \times \mathbf{E}^2$  and takes on the form ICFIE on  $\Gamma$ :

$$\begin{pmatrix} (\mu_2 + \mu_1)(2\mu_1)^{-1}I + \mu_2\mu_1^{-1}\mathcal{K}_2 - \mathcal{K}_1^{\text{per}} & -i\omega\epsilon_1\mathcal{S}_1^{\text{per}} + i\omega\epsilon_2\mathcal{S}_2 + i(\omega\mu_1)^{-1}(\mathcal{T}_1^{\text{PV,per}} - \mathcal{T}_2^{\text{PV}}) \\ i\omega\mu_1\mathcal{S}_1^{\text{per}} - i\omega\mu_2\mathcal{S}_2 + i(\omega\epsilon_1)^{-1}(\mathcal{T}_1^{\text{PV,per}} - \mathcal{T}_2^{\text{PV}}) & (\epsilon_2 + \epsilon_1)(2\epsilon_1)^{-1}I + \epsilon_2\epsilon_1^{-1}\mathcal{K}_2 - \mathcal{K}_1^{\text{per}} \end{pmatrix} \times \begin{pmatrix} \mathbf{j}_2 \\ \mathbf{m}_2 \end{pmatrix} = \begin{pmatrix} \mathbf{n} \times \mathbf{H}^i \\ \mathbf{n} \times \mathbf{E}^i \end{pmatrix} \quad (21)$$

where the wavenumbers  $k_i$  are defined as  $k_i = \omega\sqrt{\epsilon_i\mu_i}$  for  $i = 1, 2$ . For the case of smooth interfaces  $\Gamma$ , the integral operators  $\mathcal{K}_i$  and  $\mathcal{T}_1^{\text{PV,per}} - \mathcal{T}_2^{\text{PV}}$  are compact operators from  $H_{\text{div}}^{-\frac{1}{2}}(\Gamma)$  to itself. However, the

operators  $\mathcal{S}_i$  are not compact on  $H_{\text{div}}^{-\frac{1}{2}}(\Gamma)$ . Nevertheless, if one views the operator on the left-hand side of equation (21) as an operator from  $H^s(TM(\Gamma)) \times H^s(TM(\Gamma))$ , where  $H^s(TM(\Gamma))$  denotes the classical Sobolev space of tangent vector field on  $\Gamma$ , then all the operators  $\mathcal{S}_i$ ,  $\mathcal{K}_i$ , and  $\mathcal{T}_1^{\text{PV}} - \mathcal{T}_2^{\text{PV}}$  are compact.

The significant computational challenge associated with the numerical solution of equations (21) is related to the efficient evaluation of the periodic Green's function  $G_k^{\text{per}}$ . There is an extensive literature devoted to the issues related to the efficient evaluation of periodic Green's function. In what follows we present a method of solution of such integral equations based on three main elements: (1) use of windowing/cutoff functions to approximate the infinite series representations of  $G_k^{\text{per}}$  by truncated, rapidly convergent sums; (2) Taylor expansions of the terms in the series representation of  $G_k^{\text{per}}$  corresponding to  $(m^2 d_1^2 + n^2 d_2^2)^{\frac{1}{2}} > N$  that achieve a separation of the contributions of the integration points  $\mathbf{x}'$  from the contributions of the target points  $\mathbf{x}$ ; (3) high-order quadrature methods based on overlapping or non-overlapping Chebyshev patches are used to integrate the terms in the relevant integral operators corresponding to the contributions in  $G_k^{\text{per}}$  that arise from modes such that  $(m^2 d_1^2 + n^2 d_2^2)^{\frac{1}{2}} \leq N$ ; and (4) accelerated evaluations based on periodic arrays of equivalent sources and FFT convolutions.

**Truncated sums using windowing functions.** The very slow/conditional convergence of the periodic Green's function has been extensively discussed in the literature and several methods to accelerate its convergence, notably the Ewald's method, have been proposed. We propose a novel idea for fast evaluations of periodic Green's functions: we use a smooth windowing function  $\chi$  such that  $\chi(t) = 1, t \leq 1$  and  $\chi(t) = 0, t \geq 2$  and we approximate  $G_k^{\text{per}}$  in the following manner:

$$G_k^{\text{per}}(\mathbf{x}, \mathbf{x}') \approx \sum_{(md_1)^2 + (nd_2)^2 \leq 4L^2} \chi\left(\frac{d_{mn}}{L}\right) e^{i\alpha nd_1} e^{i\beta md_2} \\ \times G_k(x_1 - (x'_1 + nd_1), x_2 - (x'_2 + md_2), x_3 - x'_3) = G_k^{\text{per},L}(\mathbf{x}, \mathbf{x}'), \quad (22)$$

where  $d_{mn} = ((md_1)^2 + (nd_2)^2)^{\frac{1}{2}}$ . The following result establishes the super-algebraic convergence of  $G_k^{\text{per},L}$  to  $G_k^{\text{per}}$ :

**Theorem 2.1** (Bruno, Shipman, Turc, Venakides) *If  $k$  is not a Wood anomaly, that is if  $k^2 \neq \alpha_m^2 + \beta_n^2$  for all  $(m, n) \in \mathbb{Z} \times \mathbb{Z}$  where  $\alpha_m = \alpha + \frac{2\pi m}{d_1}$ ,  $\beta_n = \beta + \frac{2\pi n}{d_2}$ , then for all  $\mathbf{x} \neq \mathbf{x}'$  and all integers  $p$  such that  $2 \leq p$*

$$|G_k^{\text{per}}(\mathbf{x}, \mathbf{x}') - G_k^{\text{per},L}(\mathbf{x}, \mathbf{x}')| \leq CL^{\frac{1}{2}-p}.$$

Figure 7 demonstrates the excellent accuracies arising from use of Theorem 2.1.

**Separable variables representations of non-adjacent interactions.** In order to further accelerate the evaluation of  $G_k^{\text{per},L}$ , we derive Taylor series expansions of quantities  $G_k(x_1 - (x'_1 + nd_1), x_2 - (x'_2 + md_2), x_3 - x'_3)$  for  $|m|, |n| > N \gg 1$  in terms of the small parameter  $(m^2 d_1^2 + n^2 d_2^2)^{-\frac{1}{2}}$  and expressions that involve separable variables  $\mathbf{x} = (x_1, x_2, x_3)$  and  $\mathbf{x}' = (x'_1, x'_2, x'_3)$ . To this end, we introduce the notations

$$r_{mn} = ((x+m)^2 + (y+n)^2 + z^2)^{\frac{1}{2}}, \quad r_{mn}^0 = (m^2 + n^2)^{\frac{1}{2}}, \quad \hat{u}_{mn} = \frac{(m, n)}{r_{mn}^0}$$

and express

$$r_{mn} = r_{mn}^0 (1 + a_1 \alpha_1 + a_2 \alpha_2 + a_1^2 + a_2^2 + a_3^2) = r_{mn}^0 \left( 1 + \frac{1}{2} (\alpha_1 a_1 + \alpha_2 a_2) + \mathcal{O}\left(\frac{1}{(r_{mn}^0)^2}\right) \right) \\ = r_{mn}^0 + (x, y) \cdot \hat{u}_{mn}^0 + f, \quad (23)$$

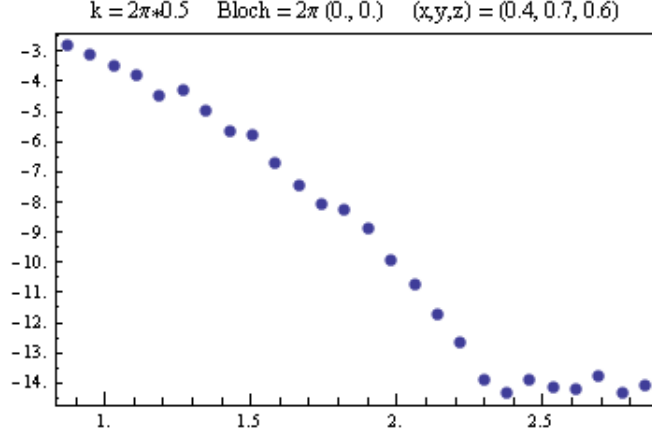


Figure 7:  $\log_{10}$  of the periodic Green function errors as a function of the  $\log_{10}$  of the number of periods  $L$  considered in the smooth truncation of the periodic Green function, according to Theorem 2.1.

where

$$a_1 = \frac{x}{r_{mn}^0}, \quad a_2 = \frac{y}{r_{mn}^0}, \quad a_3 = \frac{z}{r_{mn}^0}, \quad \alpha_1 = \frac{2m}{r_{mn}^0}, \quad \alpha_2 = \frac{2n}{r_{mn}^0}. \quad (24)$$

Using the fact that for small  $\epsilon$

$$(1 + \epsilon)^{\frac{1}{2}} = 1 + \sum_{\ell=1}^{\infty} \delta_{\ell} \epsilon^{\ell}$$

where  $\delta_1 = 1/2$  and  $\delta_{\ell+1} = -\frac{\ell-1/2}{\ell+1} \delta_{\ell}$ ,  $\ell \geq 1$  we get that

$$f = r_{mn}^0 \sum_{\ell=1}^{\infty} \delta_{\ell} (a_1 \alpha_1 + a_2 \alpha_2 + a_1^2 + a_2^2 + a_3^2)^{\ell} - \frac{1}{2} r_{mn}^0 (\alpha_1 a_1 + \alpha_2 a_2). \quad (25)$$

It follows then that

$$\begin{aligned} e^{ikr_{mn}} &= e^{ikr_{mn}^0} e^{ik(x,y) \cdot \hat{u}_{mn}^0} e^{ikf} = e^{ikr_{mn}^0} e^{ik(x,y) \cdot \hat{u}_{mn}^0} (1 + ikf - \frac{1}{2} k^2 f^2 + \dots) \\ &= e^{ikr_{mn}^0} e^{ik(x,y) \cdot \hat{u}_{mn}^0} (1 + h). \end{aligned} \quad (26)$$

Furthermore, we have

$$r_{mn}^{-1} = (r_{mn}^0)^{-1} (1 + g), \quad g = \sum_{\ell=1}^{\infty} \gamma_{\ell} (a_1 \alpha_1 + a_2 \alpha_2 + a_1^2 + a_2^2 + a_3^2)^{\ell}, \quad (27)$$

where  $\gamma_1 = -1/2$  and  $\gamma_{\ell+1} = -\frac{1/2+\ell}{\ell+1} \gamma_{\ell}$  and hence

$$\begin{aligned} \frac{e^{ikr_{mn}}}{r_{mn}} &= \frac{e^{ikr_{mn}^0}}{r_{mn}^0} e^{ik(x,y) \cdot \hat{u}_{mn}^0} (1 + g + h + gh) \\ &= \frac{e^{ikr_{mn}^0}}{r_{mn}^0} e^{ik(x,y) \cdot \hat{u}_{mn}^0} \left( 1 + \sum_{\mathbf{i}=(i_1, i_2, i_3)} (x, y, z)^{\mathbf{i}} \sum_{j=0}^{[\|\mathbf{i}\|/2]} \frac{C_{mn}^{\mathbf{i}, j}}{(r_{mn}^0)^{|\mathbf{i}\| - j}} \right) \end{aligned} \quad (28)$$

where the coefficients  $C_{mn}^{\mathbf{i},j}$  are of the form  $\frac{n^{p_1} m^{p_2}}{(r_{mn}^0)^{p_1+p_2}}$  and can be computed explicitly for all  $m, n$ . For instance, we have

$$\begin{aligned}
C_{mn}^{(1,0,0),0} &= -\frac{\alpha_1}{2}, C_{mn}^{(0,1,0),0} = -\frac{\alpha_2}{2}, C_{mn}^{(0,0,1),0} = 0 \\
C_{mn}^{(2,0,0),0} &= -\frac{1}{2} + \frac{3}{8}\alpha_1^2, C_{mn}^{(0,2,0),0} = -\frac{1}{2} + \frac{3}{8}\alpha_2^2, C_{mn}^{(0,0,2),0} = -\frac{1}{2}, C_{mn}^{(1,1,0),0} = \frac{3}{4}\alpha_1\alpha_2 \\
C_{mn}^{(2,0,0),1} &= \frac{ik}{2}(1 - \alpha_1^2/2), C_{mn}^{(0,2,0),1} = \frac{ik}{2}(1 - \alpha_2^2/2), C_{mn}^{(0,0,2),1} = \frac{ik}{2}, C_{mn}^{(1,1,0),1} = \frac{ik}{2}(1 - \alpha_1\alpha_2/2).
\end{aligned} \tag{29}$$

Consequently, we obtain that

$$\begin{aligned}
G_k(x_1 - (x'_1 + nd_1), x_2 - (x'_2 + md_2), x_3 - x'_3) &= \frac{e^{ikd_{mn}}}{4\pi d_{mn}} e^{ik(x'_1 - x_1, x'_2 - x_2) \cdot u_{mn}} \\
&\times \left( 1 + \sum_{(\mathbf{i}, \mathbf{i}') \neq (0,0)} \mathbf{x}' \mathbf{x}^{\mathbf{i}} (-1)^{|\mathbf{i}|} \binom{\mathbf{i} + \mathbf{i}'}{\mathbf{i}} \sum_{j=0}^{\frac{|\mathbf{i} + \mathbf{i}'|}{2}} \frac{C_{mn}^{\mathbf{i} + \mathbf{i}', j}}{(d_{mn})^{|\mathbf{i} + \mathbf{i}'| - j}} \right)
\end{aligned} \tag{30}$$

where

$$d_{mn} = ((md_1)^2 + (nd_2)^2)^{\frac{1}{2}}, \quad u_{mn} = \frac{(md_1, nd_2)}{d_{mn}} \tag{31}$$

and we used the classical notation  $\mathbf{x}^{\mathbf{i}} = x_1^{i_1} x_2^{i_2} x_3^{i_3}$ .

**Fast evaluations of the boundary layer potentials with periodic Green's functions.** Based on the ideas developed in the previous sections, we approximate the evaluations of the single layer potential in the following manner:

$$\begin{aligned}
\int_{\Gamma} G_k^{per}(\mathbf{x}, \mathbf{x}') \mu_{per}(\mathbf{x}') ds(\mathbf{x}') &\approx \sum_{|m|, |n| < N} \chi\left(\frac{d_{mn}}{L}\right) e^{i\alpha nd_1} e^{i\beta md_2} \\
&\times \int_{\Gamma} G_k(x_1 - (x'_1 + nd_1), x_2 - (x'_2 + md_2), x_3 - x'_3) \mu_{per}(\mathbf{x}') ds(\mathbf{x}') \\
&+ \sum_{N \leq |m|, |n| \leq 2L/d_1} \chi\left(\frac{d_{mn}}{L}\right) e^{i\alpha nd_1} e^{i\beta md_2} \frac{e^{ikd_{mn}}}{4\pi d_{mn}} e^{-ik(x_1, x_2) \cdot u_{mn}} \\
&\times \sum_{|\mathbf{i}|, |\mathbf{i}'|=0}^T I(u_{mn}, \mathbf{i}, \mu_{per})(x_1, x_2, x_3)^{\mathbf{i}'} (-1)^{|\mathbf{i}|} \binom{\mathbf{i} + \mathbf{i}'}{\mathbf{i}} \sum_{j=0}^{\frac{|\mathbf{i} + \mathbf{i}'|}{2}} \frac{C_{mn}^{\mathbf{i} + \mathbf{i}', j}}{(d_{mn})^{|\mathbf{i} + \mathbf{i}'| - j}}
\end{aligned} \tag{32}$$

where the quantities  $I(u_{mn}, \mathbf{i}', \mu_{per})$  are defined as

$$I(u_{mn}, \mathbf{i}, \mu_{per}) = \int_{\Gamma} e^{ik(x'_1, x'_2) \cdot u_{mn}} (x'_1, x'_2, x'_3)^{\mathbf{i}} \mu_{per}(\mathbf{x}') ds(\mathbf{x}'). \tag{33}$$

We obtain similar expressions for all of the other necessary boundary layer potentials in equations (21). In that case of open surfaces, the unknown integral density  $\mu_{per}$  is singular and we have  $\mu_{per}(\mathbf{x}) = \frac{\mu^{reg}(\mathbf{x})}{\omega(\mathbf{x})}$

where  $\mu^{reg}$  is a smooth function and for a point  $\mathbf{x} \in \Gamma$  the weight  $\omega(\mathbf{x}) = (d(\mathbf{x}, \partial\Gamma))^{\frac{1}{2}}$ . Thus we pose the corresponding integral equations in terms of the *smooth* density  $\mu^{reg}$  via the ansatz above. Taking into account the approximations (32), we solve the following integral equations:

$$\begin{aligned}
& \sum_{|m|,|n|<N} \chi\left(\frac{d_{mn}}{L}\right) e^{i\alpha nd_1} e^{i\beta md_2} \int_{\Gamma} G_k(x_1 - (x'_1 + nd_1), x_2 - (x'_2 + md_2), x_3 - x'_3) \frac{\mu^{reg}(\mathbf{x}')}{\omega(\mathbf{x}')} ds(\mathbf{x}') \\
& + \sum_{N \leq |m|, |n| \leq 2L/d_1} \chi\left(\frac{d_{mn}}{L}\right) e^{i\alpha nd_1} e^{i\beta md_2} \frac{e^{ikd_{mn}}}{4\pi d_{mn}} e^{-ik(x_1, x_2) \cdot u_{mn}} \\
& \times \sum_{|\mathbf{i}|, |\mathbf{i}'|=0}^T I(u_{mn}, \mathbf{i}, \mu^{reg})(x_1, x_2, x_3)^{\mathbf{i}'} (-1)^{|\mathbf{i}|} \binom{\mathbf{i} + \mathbf{i}'}{\mathbf{i}} \sum_{j=0}^{\frac{|\mathbf{i} + \mathbf{i}'|}{2}} \frac{C_{mn}^{\mathbf{i} + \mathbf{i}', j}}{(d_{mn})^{|\mathbf{i} + \mathbf{i}'| - j}} \\
& = -\exp(ik\mathbf{d} \cdot \mathbf{x}), \quad \mathbf{x} \in \Gamma
\end{aligned} \tag{34}$$

where

$$I(u_{mn}, \mathbf{i}, \mu^{reg}) = \int_{\Gamma} e^{ik(x'_1, x'_2) \cdot u_{mn}} (x'_1, x'_2, x'_3)^{\mathbf{i}} \frac{\mu^{reg}(\mathbf{x}')}{\omega(\mathbf{x}')} ds(\mathbf{x}'). \tag{35}$$

and the expressions  $u_{mn}$ ,  $d_{mn}$  and  $C_{mn}^{\mathbf{i}, j}$  are defined in the previous Section.

In order to obtain high-order discretizations of the integral operators that involve periodic Green's functions we use our previously developed strategy based on overlapping patches for the cases when the solutions of the integral equations are smooth and non-overlapping Chebyshev patches in the cases when the solutions undergo rapid transitions in the vicinity of geometric singularities. Our approach calls for (1) the evaluation of far-away smooth interactions — that is, contributions to the integrals related to integration points  $\mathbf{x}'$  that are sufficiently separated by the target points  $\mathbf{x}$  and (2) the evaluation of nearby singular interactions — that is, contributions to the integrals related to integration points  $\mathbf{x}'$  that are close to the target points  $\mathbf{x}$ . In case (2), the terms  $G_k(x_1 - (x'_1 + nd_1), x_2 - (x'_2 + md_2), x_3 - x'_3)$  are singular only for  $\mathbf{x} = \mathbf{x}'$  and  $n = m = 0$ —that is the free-space Green's function, and the singularity is resolved with high-order by polar changes of variables and interpolation techniques. The far-away interactions (1) in the case of the free-space Green's function  $G_k$  are accelerated by use of equivalent sources placed on Cartesian grids and 3D sparse FFT convolutions. These techniques extend to the case of evaluating far-away interactions via  $G_k^{L, per}$  which we describe next.

The first step of this approach consists of partitioning a cube  $C$  of size  $A$  circumscribing the scatterer into  $L^3$  identical cubic cells  $c_i$  of size adjusted (in the sense of small enough) so that they do not admit either inner acoustic resonances – eigenfunctions of the Laplacian with Dirichlet boundary conditions. The main idea of the acceleration algorithm is to seek to substitute the surface “true” sources which correspond to the discretization points contained in a certain cube  $c_i$  by acoustic periodic “equivalent sources” on the faces of  $c_i$  in a manner such that the acoustic fields generated by the  $c_i$ -equivalent sources approximate to high order accuracy the fields produced by the true  $c_i$  sources at all points in space non-adjacent to  $c_i$ . The precise concept of adjacency [2] results from requiring that the approximation corresponding to a given cell  $c_i$  be valid within exponentially small errors outside the concentric cube  $\mathcal{S}_i$  of triple size. At the heart of this method lies the use of equivalent sources which consist of acoustic monopoles and dipoles placed on three independent sets  $\Pi_{ac}^l$ , each one parallel to  $x_l = 0$ . For a fixed value  $l = 1, 2, 3$ , we associate to an acoustic field  $u$  and each cell  $c_i$ -equivalent sources, acoustic monopoles  $\xi_{i,j}^{(m)l} G_k^{L, per}(\mathbf{x} - \mathbf{x}_{i,j}^l)$  and dipoles  $\xi_{i,j}^{(d)l} \partial G_k^{L, per}(\mathbf{x} - \mathbf{x}_{i,j}^l) / \partial x_l$  placed at points  $\mathbf{x}_{i,j}^l, l = 1, \dots, M^{equiv}$  contained within certain subsets  $\Pi_i^l$  which lie within the union of two circular domains concentric with and circumscribing the faces of  $c_i$ , their radius chosen according to the prescriptions in [2]. The fields  $\psi^{c_i, true}$  radiated by the  $c_i$ -true sources

Scatterer	Unknowns	L	$\epsilon$	$\epsilon_{conv}$	It/Time
Sphere	$6 \times 16 \times 16$	20	$8.0 \times 10^{-3}$	$1.8 \times 10^{-2}$	7/3m12sec
Sphere	$6 \times 16 \times 16$	30	$1.4 \times 10^{-4}$	$1.8 \times 10^{-4}$	7/7m3sec
Sphere	$6 \times 16 \times 16$	50	$2.8 \times 10^{-5}$		7/19m33sec
Sphere(T Ac)	$12 \times 16 \times 16$	20	$2.1 \times 10^{-3}$	$8.2 \times 10^{-4}$	19/5m38sec
Sphere(T Ac)	$12 \times 16 \times 16$	30	$8.4 \times 10^{-4}$	$2.4 \times 10^{-4}$	19/9m29sec
Sphere(T Ac)	$12 \times 32 \times 32$	50	$4.9 \times 10^{-5}$		19/26m10sec
Sphere(T Diel)	$24 \times 16 \times 16$	20	$7.2 \times 10^{-4}$	$9.8 \times 10^{-5}$	103/28m23sec
Sphere(T Diel)	$24 \times 16 \times 16$	30	$6.3 \times 10^{-4}$	$8.0 \times 10^{-6}$	103/31m50sec
Sphere(T Diel)	$24 \times 32 \times 32$	50	$3.4 \times 10^{-5}$		103/44m8sec
Cube	$6 \times 16 \times 16$	20	$1.6 \times 10^{-3}$	$6.4 \times 10^{-3}$	34/7m57sec
Cube	$6 \times 16 \times 16$	30	$8.6 \times 10^{-5}$	$2.3 \times 10^{-3}$	34/11m42sec
Cube	$6 \times 16 \times 16$	50	$5.5 \times 10^{-5}$		34/53m13sec
Disc	$5 \times 16 \times 16$	20	$1.3 \times 10^{-3}$	$3.7 \times 10^{-3}$	10/4m37sec
Disc	$5 \times 16 \times 16$	30	$7.1 \times 10^{-5}$	$4.2 \times 10^{-4}$	10/8m18sec

Table 1: Convergence of the solvers using  $G_k^{L,per}$  even without use of Taylor expansions.

are approximated themselves by fields  $\psi^{c_i,eq}$  radiated by the  $c_i$ -equivalent sources

$$\psi^{c_i,eq}(\mathbf{x}) = \sum_{j=1}^{\frac{1}{2}M^{equiv}} \left( \xi_{i,j}^{(m)l} G_k^{L,per}(\mathbf{x}, \mathbf{x}_{i,j}^l) + \xi_{i,j}^{(d)l} \frac{\partial G_k^{L,per}(\mathbf{x}, \mathbf{x}_{i,j}^{(d)l})}{\partial x_l} \right). \quad (36)$$

The parameters  $n_t$ ,  $M^{equiv}$  and the unknown monopole and dipole intensities in (36) are chosen so that the truncated spherical wave expansions of order  $n_t$  for  $\psi^{c_i,true}$  and  $\psi^{c_i,eq}$  differ in no more than  $\mathcal{O}(\epsilon)$  outside  $\mathcal{S}_i$ . Based on considerations on spherical harmonics, it was required in [2] that  $M^{equiv} \gtrsim n_t^2$  equivalent sources are used for each acoustic component and the the intensities are chosen such that to minimize in the mean-square norm the differences  $(\psi^{c_i,eq}(\mathbf{x}) - \psi^{c_i,true}(\mathbf{x}))$  as  $\mathbf{x}$  varies over a number  $n^{coll}$  collocation points on  $\partial\mathcal{S}_i$ . Hence, the intensities in (36) are obtained in practice as the least-squares solution of three overdetermined linear systems  $\mathbf{A}\xi = \mathbf{b}$  where  $\mathbf{A}$  are  $n^{coll} \times M^{equiv}$  matrices. This strategy leads to a computational cost of  $\mathcal{O}(4L^2N^{4/3} \log N)$  to evaluate the boundary layer potentials involving  $G_k^{L,per}$ , where  $N$  is the number of discretization points.

Finally, the terms in equations (33) and (34) that involve separate contributions of the target point  $\mathbf{x}$  from the integration point  $\mathbf{x}'$  are computed in the following manner: (a) for all  $(m, n)$  such that  $N \leq |m|, |n| \leq 2L$  the coefficients  $C_{mn}^{i,j}$  are precomputed for all multi-indices  $\mathbf{i}$  such that  $|\mathbf{i}| \leq 2T$  and all indices  $j$  such that  $0 \leq j \leq T$  following the Taylor series algebra manipulations described in Section 3.1 and (b) for all multi-indices  $\mathbf{i}$  per part (a) the integrals  $I(u_j, \mathbf{i}, \mu_{reg})$  are computed for a number  $J$  of directions  $j$  uniformly distributed on the two-dimensional unit circle  $\mathbb{S}^1$  and the quantities  $I(u_{mn}, \mathbf{i}, \mu_{reg})$  for all  $(m, n)$  such that  $N \leq |m|, |n| \leq 2L$ , in turn, are obtained from Fourier interpolation from the values  $I(u_j, \mathbf{i}, \mu_{reg})$ ,  $j = 1, \dots, J$ —the number  $J$  is typically much smaller than  $4(2L - N)^2$ . Thus, we must choose three parameters  $N, L$ , and  $T$  in equations (34) so that we get high-order accuracy in small computational times.

## 2.4 Numerical results

In this section we present several numerical results concerning scattering off of periodic arrays of scatterers. In order to assess the accuracy of our solver, we present the energy balance, that is the energy of the incident

wave equals the energy of the reflected wave plus the energy of the transmitted wave. The energy balance can be expressed mathematically in terms of the Rayleigh coefficients (also called “efficiencies”), and it takes on the following form:

$$\sum_{(n,m) \in U} \gamma_{n,m} |B_{n,m}^+|^2 + \sum_{(n,m) \in U} \gamma_{n,m} |B_{n,m}^- + \delta_{n,m}^{0,0}|^2 = \gamma. \quad (37)$$

in the acoustic case and

$$\sum_{(n,m) \in U} \gamma_{n,m} |\mathbf{B}_{n,m}^+|^2 + \sum_{(n,m) \in U} \gamma_{n,m} |\mathbf{B}_{n,m}^- + \delta_{n,m}^{0,0}|^2 = \gamma. \quad (38)$$

in the electromagnetic case. We will present in our numerical tests the energy balance which is defined as

$$\epsilon = \frac{\left| \sum_{(n,m) \in U} \gamma_{n,m} |B_{n,m}^+|^2 + \sum_{(n,m) \in U} \gamma_{n,m} |B_{n,m}^- + \delta_{n,m}^{0,0}|^2 - \gamma \right|}{\gamma}. \quad (39)$$

In the case of transmission problems, the transmission quantity is a measure of the fraction of the energy of the incident wave which is transmitted by the periodic scatterer and it is defined as:

$$T = \frac{\sum_{(n,m) \in U} \gamma_{n,m} |\mathbf{B}_{n,m}^- + \delta_{n,m}^{0,0}|^2}{\gamma}. \quad (40)$$

We present numerical results for three geometries: spheres, cubes, and discs. The first case is treated with the overlapping method and the other two with the non-overlapping method. We present the energy balance  $\epsilon$  as well as the errors, evaluated by means of a resolution study, in the coefficient  $B_{0,0}^-$  in the sound-soft case and in  $T$  in the transmission case—we denote these errors by  $\epsilon_{conv}$ . All linear systems were solved using GMRES to a residual of  $10^{-4}$ .

We present in Table 1 the high-order nature of our solver as a function of the parameter  $L$  in the definition of  $G_k^{L,per}$ . In all of the sound soft cases the periods are  $d_1 = d_2 = 4$ , we consider normal incidence  $\psi = \phi = 0$ , the wavenumber  $k = 0.75$ . In the case of the transmission problem, we take  $\omega = 1$ ,  $\epsilon_1 = 1$ ,  $\epsilon_2 = 40$  and  $\psi = \pi/6$ ,  $\phi = 0$ . With regards to computational times, for comparison we note that the implementation one of the most advanced techniques for evaluation of periodic Green’s functions [3] (which is based on Kummer transforms, either spatial or spectral representations, supplemented by Shanks transforms) is reported to take several milliseconds per evaluation point [4]. Thus, for a discretization  $6 \times 16 \times 16$  there are about  $1.8 \times 10^6$  evaluations of periodic Green’s functions which will require at least  $1.8 \times 10^3$  seconds (30 minutes) *to evaluate just one matrix vector product*. In contrast, as it can be seen in Tables 1-4, our solvers require about 82 sec for a matrix vector product to obtain results with four digits of accuracy.

In the next three tables, Tables 2-4 we present results for the cases when Taylor expansions are used. The results concern the sound-soft case, normal incidence,  $d_1 = d_2 = 4$ . We conclude that reductions about one order in magnitude in computational times can be garnered from use of Taylor expansions, while the results are still accurate with two digits.

We present in Figure 8 the acoustic transmission coefficient as a function of the frequency  $\omega$  in the case of scattering from a periodic array of spheres with  $\epsilon_2 = 40$  and two values of the azimuthal angle  $\psi = 0$  (left) and  $\psi = \pi/6$  (center) and a periodic array of smoothed cubes ( $d=0.1$ ) (right) with normal incidence and  $\epsilon_2 = 40$ . We note that sharp transitions in the transmission curves correspond to resonant behavior — around  $\omega = 0.7$  for normal incidence and  $\omega = 0.5$  for the case of oblique incidence in the case of spheres and for  $\omega = 0.79$  in the case of smoothed cubes.

k	Unknowns	N	L	T	$\epsilon$	$\epsilon_{conv}$	It/Time
1.75	$6 \times 16 \times 16$	20	20		$2.8 \times 10^{-2}$		9/3m15sec
1.75	$6 \times 16 \times 16$	14	20	2	$5.8 \times 10^{-3}$	$3.5 \times 10^{-2}$	10/1m20sec
3.75	$6 \times 16 \times 16$	80	80		$1.9 \times 10^{-3}$		18/51m4sec
3.75	$6 \times 16 \times 16$	20	40	2	$1.4 \times 10^{-2}$	$1.3 \times 10^{-2}$	18/3m41sec
4.75	$6 \times 16 \times 16$	80	80		$1.9 \times 10^{-3}$		29/54m51sec
4.75	$6 \times 16 \times 16$	28	80	2	$5.9 \times 10^{-3}$	$2.0 \times 10^{-3}$	29/9m59sec

Table 2: Scattering by a by-periodic array of spheres;  $\epsilon$  and  $\epsilon_{conv}$  denote the energy balance error and the error in reflection/transmission evaluated by means of a convergence study. Note that use of a Taylor expansion (indicated in the table by displaying the Taylor truncation order  $T = 2$ ) significantly accelerates the solution process.

k	Unknowns	N	L	T	$\epsilon$	$\epsilon_{conv}$	It/Time
1.75	$6 \times 16 \times 16$	20	20		$9.0 \times 10^{-3}$		50/10m4sec
1.75	$6 \times 16 \times 16$	14	20	2	$2.0 \times 10^{-2}$	$4.2 \times 10^{-2}$	50/8m42sec
3.75	$6 \times 16 \times 16$	80	80		$1.3 \times 10^{-5}$		70/58m42sec
3.75	$6 \times 16 \times 16$	20	40	2	$1.9 \times 10^{-3}$	$1.9 \times 10^{-2}$	70/14m21sec
4.75	$6 \times 16 \times 16$	80	80		$5.7 \times 10^{-3}$		80/60m8sec
4.75	$6 \times 16 \times 16$	28	80	2	$9.0 \times 10^{-3}$	$2.9 \times 10^{-2}$	80/27m59sec

Table 3: Scattering by a by-periodic array of cubes; otherwise same as figure 2.

k	Unknowns	N	L	T	$\epsilon$	$\epsilon_{conv}$	It/Time
1.75	$6 \times 16 \times 16$	20	20		$4.0 \times 10^{-2}$		11/4m47sec
1.75	$6 \times 16 \times 16$	14	20	2	$1.2 \times 10^{-2}$	$4.1 \times 10^{-2}$	11/3m8sec
3.75	$6 \times 16 \times 16$	80	80		$1.4 \times 10^{-5}$		17/50m56sec
3.75	$6 \times 16 \times 16$	20	40	2	$2.0 \times 10^{-2}$	$2.4 \times 10^{-2}$	17/5m54sec
4.75	$6 \times 16 \times 16$	80	80		$6.5 \times 10^{-3}$		20/51m8sec
4.75	$6 \times 16 \times 16$	28	80	2	$2.3 \times 10^{-2}$	$4.4 \times 10^{-2}$	29/10m47sec

Table 4: Scattering by a by-periodic array of plates (see Figure 2); otherwise same as figure 2.

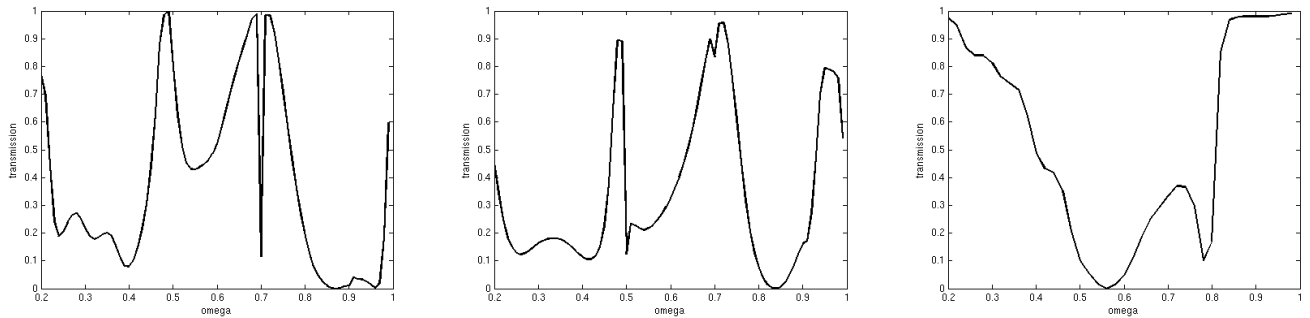


Figure 8: Transmission coefficients as a function of the frequency  $\omega$  in the case of scattering from a periodic array of spheres with  $\epsilon_2 = 40$  and  $\psi = 0$  (left) and  $\psi = \pi/6$  (center) and from a periodic array of cubes (right).

To conclude this report we return to its first image, Figure 1, which displays the dielectric transmission coefficient as a function of the frequency  $\omega$  in the case of scattering from a periodic array of spheres with  $\epsilon_2 = 40$  and normal incidence around the resonant frequency  $\omega = 0.69$ , and the fields inside and around a spherical element in a periodic array. Experiments such as these demonstrate the ability of the new solvers to produce rapidly, efficiently and accurately important physical observables such as total reflection and total transmission for challenging three dimensional photonic crystals. In view of the computational times reported above in this text, we believe these solvers are orders of magnitude faster, for a given accuracy, than all other methods available at present and, in fact, will enable solution of previously intractable problems.

### Personnel Associated with the Research Effort

Dr. Santiago Fortes, PI; Dr. Oscar P. Bruno, Dr. Catalin Turc.

### References

- [1] Bruno, O., Elling, T., Paffenroth, R. and Turc, C., *Electromagnetic integral equations requiring small numbers of Krylov-subspace iterations*, J. Comput. Phys., doi:10.1016/j.jcp.2009.05.020, (2009).
- [2] Bruno, O. P. and Kunyansky, L., *A fast, high-order algorithm for the solution of surface scattering problems: basic implementation, tests and applications*, J. Computat. Phys. **169**, 80–110 (2001).
- [3] N. Guérin, S. Enoch, and G. Tayeb, *Combined method for the computation of the doubly periodic Greens function*, Journal of Electromagnetic Waves and Applications, vol. 15, pp. 205221, 2001.
- [4] E.H. Bleszynski, M.K. Bleszynski, and T. Jaroszewicz. *Rigorous Modeling of Electromagnetic Wave Interactions with Large Dense Systems of Discrete Scatterers*, Ultra-Wideband, Short Pulse Electromagnetics **9**, p. 65, F. Sabath et al. (eds.), DOI 10.1007/978-0-387-77845-7-8, Springer, 2010.